LANGMUIR

pubs.acs.org/Langmuir Article

Induced Chirality in QDs Using Thermoresponsive Elastin-like Polypeptides

Christopher D. Lowe, Helen C. Larson,[#] Yifeng Cai,[#] Huat Thart Chiang, Lilo D. Pozzo, François Baneyx, and Brandi M. Cossairt*

Cite This: *Langmuir* 2025, 41, 1047−1056 Read Online

ACCESS | Metrics & More | Article Recommendations | Supporting Information

ABSTRACT: Circular dichroism (CD) spectroscopy has emerged as a potent tool for probing chiral small-molecule ligand exchange on natively achiral quantum dots (QDs). In this study, we report a novel approach to identifying QD−biomolecule interactions by inducing chirality in CdS QDs using thermoresponsive elastin-like polypeptides (ELPs) engineered with C-terminal cysteine residues. Our method is based on a versatile two-step ligand exchange process starting from monodisperse oleate-capped QDs in nonpolar media and proceeding through an easily accessed achiral glycine-capped QD intermediate. Successful conjugation of the ELPs onto the QDs is confirmed by the diagnostic CD response corresponding to the QD electronic transitions in the visible range. The resulting ELP:CdS conjugates demonstrate thermally reversible coacervation, as observed through dynamic light scattering, small-angle X-ray scattering, and electron microscopy. This research provides a foundation for using induced chirality in QD electronic transitions to probe QD conjugation to complex peptides and proteins, opening pathways for designing dynamic, stimuli-responsive hybrid nanomaterials.

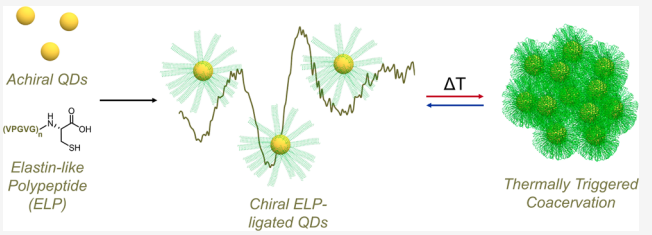

INTRODUCTION

Circular dichroism (CD) has emerged as a powerful spectroscopic probe for studying chiral small molecules as surface ligands on quantum dots (QDs). In 2013, Tohgha et al. demonstrated that absorbance and luminescence chirality could be induced on achiral and hydrophobic CdSe QDs by postsynthetic ligand exchange with L- and D-cysteine.[1,2] While the origin and mechanism of this induced chirality are still not wholly understood, two theories have been introduced to explain this phenomenon. The first is a physical distortion of the QD lattice through chiral ligand coordination to surface metal ions.[3−5] The second is the hybridization of the QD hole wave function and molecular orbitals of the ligands, which splits the electron excitation into two sublevels, as evident in the CD spectrum.[2,6,7]

While there are examples using CD to confirm chiral ligand exchanges on achiral QDs, this technique has seldom been used to confirm the conjugation of complex ligands, such as polypeptides and proteins, on QDs. Previous reports have demonstrated the ligand exchange of CdSe and CdS QDs with peptides,[8] poly-N-substituted glycines,[9,10] and DNA[11] in aqueous environments but relied on UV−vis absorbance, photoluminescence, and nuclear magnetic resonance spectroscopies to confirm conjugation. QDs are used increasingly in applications for biological systems, including bioimaging,[12] disease detection,[13] drug delivery,[14] and site-selective DNA scission,[15] highlighting the importance of understanding the interaction of the QD surface with its biological environment.

Drawing inspiration from tropoelastin, water-soluble elastin-like polypeptides (ELPs) are genetically engineered, low-complexity proteins consisting of a repeated sequence of five amino acids (valine, proline, glycine, X, and glycine) (VPGXG), where X is any amino acid except proline.[16,17] The identity of this guest residue and the number of repeated pentamers both impact the phase-transition temperature (T_t),[18] above which ELPs reversibly collapse into phase-segregated liquid droplets known as coacervates. Adding to their thermoresponsiveness, ELPs can be engineered with a variety of terminal amino acids,[19] making them attractive for drug delivery,[20] metal removal,[21] protein purification,[22] and tissue engineering.[23]

Leveraging ELP's stimuli-responsiveness and sequence-defined chemistry to coordinate inorganic nanoparticles exhibiting unique electronic and spectroscopic characteristics enables the rational design of dynamic hybrid nanomaterials.[24] While there are examples of QDs in biologically relevant environments,[25] there are few examples of cadmium chalcogenide QDs with ELPs. In 2010, Fahmi et al. demonstrated a colloidal bottom-up synthesis of CdSe with

Received: October 30, 2024
Revised: December 22, 2024
Accepted: December 22, 2024
Published: December 31, 2024

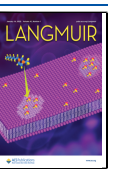

https://doi.org/10.1021/acs.langmuir.4c04339
Langmuir 2025, 41, 1047−1056

ELPs, which made QD-decorated nanofibrils that could permeate cell membranes and demonstrated no cytotoxicity.[26] In 2011, Biswas et al. described the postsynthetic conjugation of a protein containing an ELP domain to QDs that were used to image cellular processes.[27] However, neither study reported on the surface interaction of the ELP with the QD or the thermoresponsiveness of the resulting ELP-QD conjugates.

Recently, an ELP with the sequence $(VPGVG)_{96}C$ (referred to as V96-Cys) was shown to decorate gold nanoparticle surfaces and form particle-dense coacervates at elevated temperatures, which led to a plasmonic shift of the gold nanoparticles.[28] Due to the low complexity, lack of internal amino acid binding groups, and C-terminal cysteine of V96-Cys, this polypeptide also provides a platform, for the first time, for ligand exchange onto achiral CdS QDs. Additionally, by engineering a second ELP sequence with the same binding group and a shorter amino acid sequence $(VPGVG)_{54}C$ (referred to as V54-Cys), we can gain a better understanding of how the ligand length in the hybrid systems impacts their thermoresponsiveness. Finally, because both sequences contain one amino acid binding residue, we can extend the principles of postsynthetically-induced chirality in CdS QDs to include polypeptides for the first time.

Here, we describe a simple two-step method for the synthesis and characterization of V96-Cys:CdS and V54-Cys:CdS QD conjugates at μM concentrations and mild pH conditions in aqueous systems starting from traditional hydrophobic CdS QDs. We use CD spectroscopy to probe the surface interaction of the C-terminal cysteine of the ELP with CdS QDs and examine the pH dependence of their CD spectra. We then examine the dynamic thermoresponsive coacervation of hybrid ELP:QD conjugates using CD, dynamic light scattering (DLS), small-angle X-ray scattering (SAXS), and electron microscopy. To the best of our knowledge, this is the first example of postsynthetically inducing chirality in QDs using polypeptides. Additionally, for the first time, we demonstrate the thermoresponsiveness of ELP:CdS as the resulting hybrids show dynamic and cyclable coacervation, where both the polypeptide and QD undergo a spatial rearrangement in solution with structure dictated by the sequence lengths of the ELP.

EXPERIMENTAL SECTION

Materials. Oleic acid (90%), tetramethylthiourea (98%), tetramethylammonium hydroxide (1 M aqueous), glycine (98%), *N*-acetyl-L-cysteine (≥99%), L-cysteine (97%), L-cystine (99.7%), L-cysteine methyl ester hydrochloride (≥95%), Tris(2-carboxyethyl)phosphine hydrochloride (≥98%), methanol (≥99.9%), and toluene (≥99.8%) were purchased from MilliporeSigma and used without further purification. Sodium hydroxide (1 N aqueous) was purchased from Thermo Fisher and used without further purification. Dowtherm was purchased from Dow Inc. and used without further purification. Hexadecane (99%) was purchased from MilliporeSigma, dried over calcium chloride, distilled, and stored in a glovebox. Cadmium oleate was synthesized following a literature procedure.[29] 18.2 MΩ water was collected from an EMD Millipore purification system. UV−vis spectra were collected on a Cary 60 spectrophotometer from Agilent. Photoluminescence spectra were collected on a Horiba Scientific FluoroMax-4 spectrofluorometer.

Synthesis of $(VPGVG)_{54}$-Cys and $(VPGVG)_{96}$-Cys ELPs. The construction of plasmid pET25(+)-ELP(V96), which encodes V96-Cys, was previously described.[30] The gene encoding V54-Cys was obtained as a truncated PCR amplification product during the construction of pET25(+)-ELP(V96). It was inserted into pET25(+) to produce pET25(+)-ELP(V54). Plasmids were introduced into *E. coli* BL21(DE3) cells, and proteins were expressed and purified as described[28] and stored at 4 °C.

Synthesis of Oleate:CdS. The synthesis of CdS QDs was adapted from Hamachi et al.[29] Cadmium oleate (1.287g, 1.9 mmol), oleic acid (1.3 mL, 4.1 mmol), and hexadecane (60 mL) were added to a dried three-necked 250 mL round-bottomed flask equipped with a stir bar, thermowell, reflux condenser, and rubber septum. The flask was evacuated at 90 °C for 1 h. Next, the flask was put under dynamic nitrogen and heated to 230 °C. Under a nitrogen atmosphere, tetramethylthiourea (TMTU, 0.2075 g, 1.6 mmol) was dissolved in Dowtherm (3.0 mL). The TMTU solution was rapidly injected into the cadmium oleate solution and allowed to react for 3 h until there were no UV−vis absorbance changes. The temperature was then lowered to 120 °C, the condenser was quickly replaced with a distillation arm equipped with a 250 mL round-bottomed flask, and the solvent was removed via vacuum distillation. Once cooled to room temperature, in air, minimal toluene was added, and the solution was transferred to centrifuge tubes followed by precipitation with methanol (3:1 methanol:toluene) and centrifugation at 8,000 rpm for 10 min. The supernatant was discarded, and the yellow pellet was redissolved in minimal toluene. This process was repeated for 3 precipitation and centrifugation cycles. The pellet was then suspended in 10 mL of toluene and centrifuged at 8,000 rpm for 10 min. The yellow supernatant was then decanted away and stored in a vial in air. The QDs were characterized by an absorption maximum at 461 nm and were 4.8 ± 0.4 nm in diameter via TEM analysis.

Synthesis of Glycine:CdS. The synthesis of glycine:CdS was adapted from Tohga et al.[1] The concentration of QDs was determined using the Peng sizing curve.[31] To a vial, oleate:CdS (10 nmol) was added and dried. In a separate vial, glycine (0.589 g, 7.8 mM) was added with aqueous tetramethylammonium hydroxide (TMAOH, 3 mL, 1 M) and stirred at room temperature for 10 min. The TMAOH solution was then added to the QD solid, and the mixture was stirred vigorously in the dark for 24 h. To this solution, 3 mL of toluene was added and the mixture was vigorously stirred. This solution was centrifuged at 8,000 rpm for 10 min, producing a slightly yellow organic layer and a dark-yellow bottom layer. The top layer was removed, and 3 mL of toluene was added, followed by vortex mixing. This washing and centrifugation process was repeated for 3 total cycles. The resulting solution was then centrifuged using a 15,000 kDa centrifuge filter and centrifuged at 5,000 rpm for 10 min. The colorless filtrate was discarded, and 2 mL of 18 MΩ water was added to the QD solution. This centrifuge filtration process was repeated 3 times. The resulting QDs show an absorption maximum at 455 nm and were 4.11 ± 0.4 nm in diameter via TEM analysis.

Synthesis of V96-Cys:CdS and V54-Cys:CdS. The concentration of glycine:CdS QDs was determined using the Peng sizing curve.[31] $(VPGVG)_{96}C$ or $(VPGVG)_{54}C$ (V96-Cys, V54-Cys, 0.5 μmol) was dissolved in 18 MΩ water (1.5 mL). In a separate vial, a solution of Tris(2-carboxyethyl)phosphine hydrochloride (TCEP·HCl, 67.1 mg, 0.234 mmol) in 18 MΩ water (1 mL) was prepared. The TCEP·HCl solution (21.4 μL, 5 μmol) was then added to the V96-Cys or V54-Cys solutions, and the mixture was stored at 4 °C for 1 h. Next, glycine:CdS QDs (387 μL, 1.4 nmol) were added to the ELP solutions and diluted with water (591 μL). The solutions were then pH adjusted with TMAOH (200 μL, 1 M) until the pH was 11. These solutions were stored in the dark at 4 °C overnight. After overnight incubation, the QD solutions were heated to 45 °C for 20 min and centrifuged at 5,000 PM for 10 min. The resulting colorless supernatant was discarded, and the yellow pellet was dissolved in chilled 18 MΩ water (2 mL). The heat centrifugation was repeated for 2 cycles, and the resulting pellet was dissolved in 2 mL of 18 MΩ water and transferred to a prepared Float-A-Lyzer dialysis device. The solutions were dialyzed against 500 mL of 18 MΩ water. The water was replaced at 2 and 4 h before leaving overnight in 1 L of 18 MΩ water. The dialyzed samples were then lyophilized overnight, and the resulting yellow solid was dissolved in 18 MΩ water (2.5 mL) and stored in the dark at 4 °C unless used for analysis. [V96-Cys:CdS] 0.180 μM and [V54-Cys:CdS] 0.310 μM were calculated from the Peng sizing curve.[31]

https://doi.org/10.1021/acs.langmuir.4c04339
Langmuir 2025, 41, 1047−1056

Synthesis of *N*-Acetyl-L-cysteine (NAC):CdS. Samples were prepared in a manner similar to that for V96-Cys:CdS and V54-Cys:CdS QD. First, NAC (9.1 mg, 56 μmol) was dissolved in 18 MΩ water (10 mL). Next, TCEP·HCl (67.1 mg, 0.234 mmol) was prepared in 18 MΩ water (1 mL). The NAC solution (89.3 μL, 0.5 μmol) was then added to a new vial, followed by the addition of the TCEP solution (21.4 μL, 5 μmol) and storage at 4 °C for 1 h. After 1 h, glycine:CdS QDs (221 μL, 1.4 nmol) and additional 18 MΩ water (1.968 mL) were added, followed by TMAOH (200 μL, 1 M) and storage at 4 °C overnight. After incubation, the solution was centrifuged at 8,000 rpm for 10 min. The supernatant was then transferred to a 30 kDa centrifuge filter and centrifuged at 8,000 rpm for 5 min. The colorless filtrate was discarded, and 18 MΩ water was added to the QD solution; it was centrifuged again at 8,000 rpm for 5 min. This process was repeated for 5 cycles. After the 5th cycle, 18 MΩ water (2.3 mL) was added back to the final solution and was stored at 4 °C in the dark unless being used for analysis. [NAC:CdS] 0.180 μM was calculated from the Peng sizing curve.[31]

Synthesis of L-Cysteine (L-Cys):CdS QDs. Samples were prepared in a manner similar to that of V96-Cys:CdS and V54-Cys:CdS QD. First, L-Cys (5.5 mg, 45 μmol) was dissolved in 18 MΩ water (10 mL). Next, TCEP·HCl (18.2 mg, 0.0635 mmol) was prepared in 18 MΩ water (1 mL). The L-Cys solution (112 μL, 0.5 μmol) was then added to a new vial, followed by the addition of the TCEP solution (78.7 μL, 5 μmol) and storage at 4 °C for 1 h. After 1 h, glycine:CdS QDs (420 μL, 1.4 nmol) and additional 18 MΩ water (1.681 mL) were added, followed by TMAOH (200 μL, 1 M) and storage at 4 °C overnight. After incubation, the solution was centrifuged at 8,000 rpm for 10 min. The supernatant was then transferred to a 30 kDa centrifuge filter and centrifuged at 8,000 rpm for 5 min. The colorless filtrate was discarded, and 18 MΩ water was added to the QD solution, which was centrifuged again at 8,000 rpm for 5 min. This process was repeated for 5 cycles. After the 5th cycle, 18 MΩ water (2.3 mL) was added back to the final solution and was stored at 4 °C in the dark unless being used for analysis. [L-Cys:CdS] 0.400 μM was calculated from the Peng sizing curve.[31]

Synthesis of L-Cysteine Methyl Ester (L-Cys-Me):CdS QDs. Samples were prepared in a manner similar to that for V96-Cys:CdS and V54-Cys:CdS QD. First, L-Cys-Me·HCl (9.6 mg, 56 μmol) was dissolved in 18 MΩ water (10 mL). Next, TCEP·HCl (18.2 mg, 0.0635 mmol) was prepared in 18 MΩ water (1 mL). The L-Cys-Me solution (87.7 μL, 0.5 μmol) was then added to a new vial, followed by the addition of the TCEP solution (78.7 μL, 5 μmol) and storage at 4 °C for 1 h. After 1 h, glycine:CdS QDs (420 μL, 1.4 nmol) and additional 18 MΩ water (1.714 mL) were added, followed by TMAOH (200 μL, 1 M) and storage at 4 °C overnight. After incubation, the solution was centrifuged at 8,000 rpm for 10 min. The supernatant was then transferred to a 30 kDa centrifuge filter and centrifuged at 8,000 rpm for 5 min. The colorless filtrate was discarded, and 18 MΩ water was added to the QD solution, which was centrifuged again at 8,000 rpm for 5 min. This process was repeated for 5 cycles. After the 5th cycle, 18 MΩ water (2.3 mL) was added back to the final solution and was stored at 4 °C in the dark unless being used for analysis. [L-Cys-Me:CdS] 0.390 μM was calculated from the Peng sizing curve.[31]

Synthesis of L-Cystine (L-Cys-Cys):CdS QDs. The synthesis of L-Cys-Cys:CdS was adapted from Tohga et al.[1] The concentration of QDs was determined using the Peng sizing curve.[31] To a vial, oleate:CdS (6.9 nmol) was added, followed by drying. In a separate vial, L-cystine (L-Cys-Cys, 0.075 g, 0.31 mM) was added with TMAOH (2 mL, 1 M) and stirred at room temperature for 10 min. The TMAOH solution was then added to the QD solid and stirred vigorously in the dark for 24 h. To this solution, 3 mL of toluene was added and vigorously stirred. This solution was centrifuged at 8,000 rpm for 10 min, producing a slightly yellow organic layer and a dark-yellow bottom layer. The top layer was removed, and 3 mL of toluene was added, followed by vortex mixing. This washing and centrifugation process was repeated for 3 total cycles. The resulting solution was then centrifuged using a 15,000 kDa centrifuge filter and centrifuged at 8,000 rpm for 5 min. The colorless filtrate was discarded, and 2 mL of 18 MΩ water was added to the QD solution. This centrifuge filtration process was repeated 5 times. After the 5th cycle, 18 MΩ water (2.3 mL) was added back to the final solution and was stored at 4 °C in the dark unless being used for analysis. [L-Cys-Cys:CdS] 0.290 μM was calculated from the Peng sizing curve.[31]

Circular Dichroism. Spectra were collected on a Jasco J-720 spectrophotometer equipped with a temperature controller from Jasco. Scan rate: 100 nm; data pitch: 1 nm; bandwidth: 10 nm; and path length: 1 cm.

DLS Analysis. Dynamic light scattering (DLS) measurements were performed on a Malvern Zetasizer Nano ZS instrument with an 800 nm laser. The extinction coefficient used was for bulk CdS for all samples, and the refractive index used was for water in all samples except oleate:CdS samples. Scattering data were fit by using a multipeak model in the Malvern Zetasizer software.

TEM Preparation and Analysis. TEM images were collected on a FEI Tecnai G2 F20 SuperTwin microscope operated at 200 keV for bright field, cryo, and STEM. Solutions of ligand:CdS were prepared for TEM grid preparation by diluting by a factor of 2 from the solutions used for CD and SAXS. Room-temperature samples were prepared by drop-casting 5 μL of ligand:QD in water (or toluene for native oleate-capped QDs) onto a suspended TEM grid, which was then allowed to dry fully (10 min) and placed under vacuum overnight. To prepare TEM grids at 45 °C, the V54-Cys:QD solution was placed in a 45 °C chamber for 4 min (solution becomes turbid), and 5 μL was drop-cast onto a suspended TEM grid, which was then allowed to dry in the warm 45 °C chamber (5 min) and placed under vacuum overnight. TEM size analysis was performed using manual analysis in ImageJ based on images from at least 2 different grid locations and over 300 particle diameter measurements per sample. Cryogenic TEM samples were prepared using a Vitrobot Mark IV system, with liquid ethane as the coolant. Samples were prepared as above, incubated on a hot plate at 45 °C, and drop-cast onto C-flat grids. Imaging was performed using the Gatan CT3500 single-tilt liquid-nitrogen cryo-transfer holder.

SAXS Analysis. SAXS was performed on a Xenocs Xeuss 3.0 (Grenoble, France) instrument with an X-ray energy of 8.04 keV (wavelength 1.54 Å) using a Cu Kα microfocus source. Data was collected in two configurations: mid q (0.007−0.020 $Å^{-1}$) for 30 min and high q (0.020−0.200 $Å^{-1}$) for 15 min. Samples were loaded into a 1.5-mm-diameter thin-walled quartz capillary purchased from Charles Supper (Westborough, MA, USA). The Peltier stage provided by Xenocs was used to vary the temperature of the samples. Background subtraction was performed by subtracting the scattering of water measured using the same configurations. Data reduction and merging were performed using XSCAT software (Xenocs Inc.). Data fitting was performed using either Sasview (http://www.sasview.org/) or McSAS.[32]

RESULTS AND DISCUSSION

Glycine:CdS QD Ligand Exchange. Typical CdS QD synthesis schemes use long-chain fatty acid ligands and have been optimized to control the size, morphology, and optical properties of the nanocrystals.[31,33,34] Therefore, postsynthetic ligand exchange is generally required to produce high-quality water-soluble QDs. These ligand exchanges commonly use basic conditions (pH > 11) and alkyl ammonium cations.[1,2,6,35−39] Base is necessary to deprotonate the desired binding groups on the aqueous ligand, while alkyl ammonium is believed to play a key role in reducing the hydrophilicity of the anionic aqueous ligand to allow for the exchange.[39]

Unfortunately, using alkyl ammonium hydroxides is detrimental to exchanging hydrophobic QD ligands directly with proteins, as basic conditions can disrupt the hydrogen bonding network and alkyl ammonium cations are potent protein precipitating agents in the Hoffmeister series.[40,41] To circumvent these issues, exchange methods have been designed

https://doi.org/10.1021/acs.langmuir.4c04339
Langmuir 2025, 41, 1047−1056

to replace hydrophobic ligands with short-chain linkers, which are then covalently attached to polypeptides or proteins containing polydentate binding groups.[42−45]

In this study, we avoided ELP precipitation by solubilizing native oleate-capped CdS QDs (oleate:CdS) in an aqueous solution of glycine and tetramethylammonium hydroxide (TMAOH) using a method adapted from Tohgha et al.[1,2] (see the methods). Glycine was chosen as the intermediate ligand because it is a simple achiral amino acid. After the glycine ligand exchange, transmission electron microscopy (TEM) sizing analysis shows slight etching of the QDs from 4.8 to 4.1 nm in diameter (Figure 1), which has been

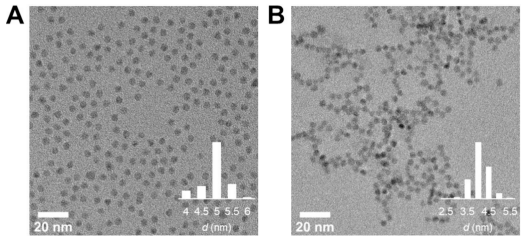

Figure 1. (A) TEM image of oleate:CdS with an average diameter of 4.8 ± 0.4 nm. (B) TEM image of glycine:CdS at pH 7 with an average diameter of 4.1 ± 0.4 nm.

previously observed in aqueous ligand exchanges.[9,10,38] This size decrease is also observed in the UV−vis absorbance and photoluminescence spectra of the glycine-capped CdS QDs (glycine:CdS) (Figures S1 and S2). Importantly, there is no CD response in the visible region of the spectrum corresponding to the QD absorbance because of the achiral QDs and achiral glycine (Figure 2A-1).

ELP Ligand Exchange. To exchange the achiral glycine ligands with ELPs terminated by a chiral Cys residue, glycine:CdS was incubated with 200 μM V96-Cys or V54-Cys at 4 °C for 24 h with TMAOH and the reducing agent tris(2-carboxyethyl)phosphine hydrochloride (TCEP·HCl) (see methods). The incubated QDs show a CD response in the visible range in as little as 1 h, but the intensity and line shape do not significantly change from 3 to 24 h, signifying that ligand exchange has gone to completion within 3 h (Figures S3 and S4). The TMAOH and TCEP·HCl are removed through dialysis, and the purified ELP:CdS aqueous solutions exhibit a strong CD signal (Figure 2A-2,3). The chiral response in the visible region corresponds to the visible QD absorbance (Figure 2B) and indicates interactions of the chiral ELP with the surface of the QD. As mentioned before, the starting glycine:CdS shows no CD signal (Figure 2A-1), and the molecular chirality of the ELP itself appears in the ultraviolet region of the CD spectrum (Figures S5 and S6). Therefore, through CD, we can conclude that ELP is present on the surface of the QD. Additionally, the QDs maintain their absorption features and band edge emission with increased trap-state emission after exchanging glycine:CdS samples with V96-Cys and V54-Cys (Figure S7).

While UV−vis and photoluminescence spectroscopies can indicate the successful exchange of QDs into the aqueous layer of a biphasic solution, they do not offer insight into the QD−ligand interface. Beyond signifying successful chiral ligand exchange, CD can provide important information about the surface interaction of complex polypeptides with the QDs. The sequence of the ELP was designed with a C-terminal cysteine

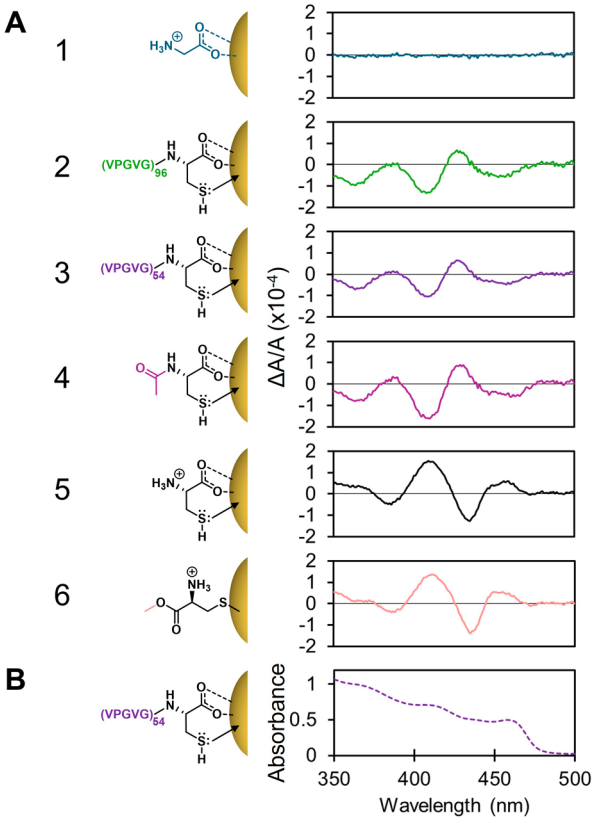

Figure 2. (A) Normalized CD spectra at pH 7 of glycine:CdS (blue, 1), V96-Cys:CdS (green, 2), V54-Cys:CdS (plum, 3), NAC:CdS (magenta, 4), L-Cys:CdS (black, 5), and L-Cys-Me:CdS (orange, 6). (B) UV−vis absorbance spectrum of V54-Cys:CdS (plum). Binding modes were assigned based on pK_a values. All CD spectra were normalized by the absorbance at the lowest-energy electronic transition.

residue to bind to the QD. To investigate the binding of the ELP to the QD, three molecular analogs exemplifying possible cysteine coordination motifs were exchanged onto the surface of glycine:CdS: *N*-acetyl-L-cysteine (NAC), L-cysteine (L-Cys), and L-cysteine methyl ester (L-Cys-Me). NAC (Figure 2A-4) was used to model an ELP bound to the QD through a C-terminal cysteine, L-Cys (Figure 2A-5) was used to model free L-Cys bound to the QD, and L-Cys-Me (Figure 2A-6) was used to model an ELP bound through an N-terminal cysteine residue. Importantly, all three analogue:CdS samples were prepared using a procedure analogous to that for the ELP samples (see methods).

The normalized CD spectra of V96-Cys:CdS and V54-Cys:CdS closely resemble the spectra of NAC:CdS but have inverted chirality relative to those of the L-Cys:CdS and L-Cys-Me:CdS samples (Figure 2A). The CD line shape is identical for the ELP-Cys:CdS and NAC:CdS systems, signifying the same surface interaction for NAC and the C-terminal cysteine on the ELP. This is expected because the amine group of the ELP C-terminal cysteine is participating in an amide bond and is less available to interact with the QD, so NAC is a more appropriate molecular analog than L-Cys and L-Cys-Me. The CD sign inversion for ELP:CdS compared to L-Cys-Me and L-Cys:CdS is expected based on previous work by Choi et al., who demonstrated that NAC:CdS and L-Cys:CdS have inverted chirality, while L-Cys and L-Cys-Me have the same CD line shape.[35] While the cause of this inversion is not fully

https://doi.org/10.1021/acs.langmuir.4c04339
Langmuir 2025, 41, 1047−1056

understood, Choi and co-workers used simulations to propose that the carbonyl of the acetyl group acts as an L-type ligand on the surface of CdSe, which causes the CD inversion of NAC compared to L-Cys and L-Cys-Me.[35] Previous findings and the results reported here suggest that the chiroptical response of QDs could selectively report on N-terminal cysteine coordination in a protein containing multiple cysteines. This is because only the N-terminal cysteine contains an amine on the nearest chiral carbon that is not an amide (Figure 3).

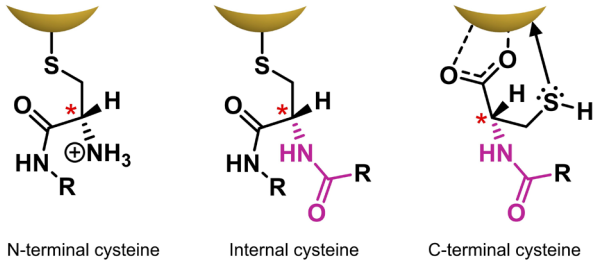

Figure 3. Hypothetical binding modes of a protein containing cysteine at the N-terminus, internal, and C-terminus positions at pH 7.

The precise assignment of ligand binding modes by CD is challenging. This is highlighted by the lack of observable change in line shape between L-Cys:CdS and L-Cys-Me:CdS at pH 7 (Figure 2A-5 and A-6). L-Cys-Me does not have a carboxylate group available to bind to the QD, unlike L-Cys, but contains a thiol with a pK_a value of 6.5.[46] At pH 7, we presume L-Cys-Me to be predominately a thiolate species, whereas the L-Cys thiol has a pK_a value of 8.7[46] and is presumed to remain predominately in the thiol form. It should be noted that the amines of both L-Cys and L-Cys-Me are likely in a dynamic L-type ligand binding equilibrium, adding an anchoring point on the QD surface based on previous work.[47,48] The lack of CD line shape differences between L-Cys:CdS and L-Cys-Me:CdS demonstrates the shortcomings of CD when probing thiolate vs carboxylate binding modes of chiral ligands with primary amines on their α-carbons. While NMR and infrared spectroscopies were useful in elucidating binding modes of L-Cys in these studies, the concentration of L-Cys (>1 mM) is almost an order of magnitude greater than the concentration of ELP in our samples, which is limited by the solubility of the polypeptides. Additionally, the NMR experiments in these studies were performed at pH values greater than 11, which makes direct comparisons to our systems at pH 7 challenging.

To support the carboxylate binding assignment of V96-Cys:CdS and V54-Cys:CdS at pH 7, as shown in Figure 2, we investigated bidentate carboxylate and thiolate vs monodentate carboxylate X-type binding modes using CD. To do this, we examined the line shapes of L-cystine (L-Cys-Cys):CdS vs L-Cys:CdS at pH 11 to induce deprotonation of the L-cysteine thiol (pK_a of 8.3).[46] L-Cys-Cys, the disulfide dimer of L-cysteine, contains two carboxyl groups but lacks the thiol group of L-cysteine. Exchanging L-Cys-Cys onto glycine:CdS proved unsuccessful, as judged by the absence of changes in the CD spectra after 24 h of incubation. However, exchanging oleate:CdS with L-Cys-Cys using a procedure adapted from Tohgha et al.[1,2] (see methods) produces chiral samples with slightly red-shifted absorbance spectra compared to L-Cys exchanged onto glycine (Figure S8A,B) (462 nm for L-Cys-Cys:CdS vs 455 nm for L-Cys:CdS, a difference that we attribute to the distinct ligand exchange methods used in the preparation of the two samples). After purification, pH adjustment, and correcting for the wavelength of the lowest-energy electronic transition, the peak locations and sign of the CD line shape in the L-Cys-Cys:CdS spectrum match L-Cys:CdS at pH 11 (Figure S8C), indicating a lack of CD line shape dependence on thiolate binding modes. These findings are also consistent with recent computational work by Han et al.,[7] which predicts no changes in the line shape of the CD spectra between a carboxylate-only binding mode and a thiolate-carboxyl binding mode of L-Cys. Therefore, the primary carboxylate binding modes of V96-Cys and V54-Cys at pH 7 are rationalized in our study using pK_a values of the thiol (9.4) and carboxyl (3.1) groups of NAC, respectively.[49] Notably, carboxylate binding has been proposed for Cd^{2+} in NAC:Cd complexes in aqueous solutions at pH 7.5, while at pH 11, all Cd^{2+} ions were bound to thiolates.[50]

In our study, we found that ligands containing thiolate groups exchange readily onto glycine:CdS at pH 11, which can be rationalized by the computations of Han and co-workers, who calculated a 0.11 eV adsorption energy difference favoring thiolate and carboxyl adsorption to CdSe over carboxylate-only adsorption.[7] These previous studies and our observation that L-Cys-Cys does not exchange with glycine while L-Cys does at pH 11 demonstrate that ligand exchange from glycine becomes more favorable with ligands containing thiolate groups. We attribute this behavior to the thermodynamic favorability of thiolate−cadmium bonds versus carboxylate−cadmium bonds. For these reasons, we hypothesize that the C-terminal cysteines of V96-Cys and V54-Cys provide thiolate groups at pH 11 that drive exchange with glycine on the surface of glycine:CdS.

To gain insight into the role of pH in determining the line shape of the CD spectra of these samples, we aimed to probe the protonation state of the thiol in V96-Cys:CdS, V54-Cys:CdS, and NAC:CdS (Figure 4A). Purified samples of V96-

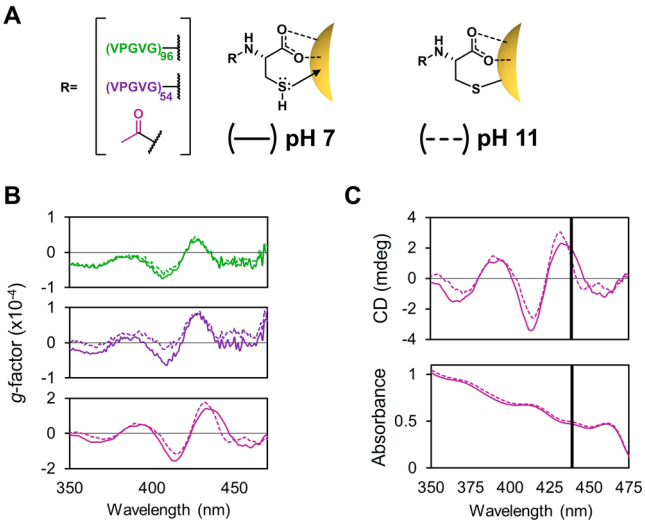

Figure 4. (A) Hypothesized primary binding modes at pH 7 (solid) and 11 (dashed). (B) *g*-factor spectra of purified V96-Cys:CdS (green), V54-Cys:CdS (purple), and NAC:CdS (plum). (C) CD spectra of purified NAC:CdS at pH 7 (solid) and 11 (dashed) and UV−vis of NAC:CdS at pH 7 (solid) and 11 (dashed). Purified samples were pH adjusted with NaOH and TCEP·HCl.

https://doi.org/10.1021/acs.langmuir.4c04339
Langmuir 2025, 41, 1047−1056

Cys:CdS, V54-Cys:CdS, and NAC:CdS were pH adjusted using TCEP·HCl and sodium hydroxide (NaOH) (see the SI). First, TCEP·HCl was added to the samples to minimize disulfide bond formation, followed by NaOH addition until the solutions reached pH 11. The dissymmetry factors (*g*-factors; see the SI for the method) were then plotted at pH values above and below the pK_a of the thiol (Figure 4B). In general, when probing the protonation state of the thiol, we observed a modest change in the *g*-factor magnitudes at different wavelengths that was more prominent in the case of NAC:CdS and V54-Cys:CdS versus the V96-Cys:CdS sample (Figure 4B). Interestingly, for NAC:CdS, the decrease in the *g*-factor magnitude around 450 nm when comparing the pH 7 (solid) and pH 11 (dashed) spectra was notable. Overlaying the CD and UV−vis spectra of NAC:CdS suggests a sharpening of the derivative-shaped CD transition corresponding to the second lowest energy electronic transition of the QD at pH 11 as highlighted by the black vertical line (Figure 4C). Previous work by Owen has demonstrated that the second electronic transition is sensitive to surface chemistry,[51] and we hypothesize that X-type thiolate binding vs L-type thiol binding can explain the sharpness in this transition at pH 11. Since similar changes are observable in V54-Cys:CdS but are less evident in V96-Cys:CdS, we propose that the steric bulk associated with the longer V96 peptide chain impedes ligand rearrangement on the surface of the QDs due to the sizable entropic barrier that would need to be overcome.

To understand the impact of pH on the chirality of V96-Cys:CdS, V54-Cys:CdS, and NAC:CdS, the magnitudes of the average *g*-factors centered around the wavelength of the most intense transition (418 nm for ELP:CdS and 423 nm for NAC:CdS) were determined (Table 1). From this data, there

Table 1. pH-Dependent Average *g*-Factors of ELP:CdS and NAC:CdS Samples at Their Most Intense Responses

	$\lvert g^+ - g^- \rvert/2_{\text{pH 11}}$	$\lvert g^+ - g^- \rvert/2_{\text{pH 7}}$
V96-Cys:CdS (418 nm)	0.5×10^{-4}	0.6×10^{-4}
V54-Cys:CdS (418 nm)	0.5×10^{-4}	0.7×10^{-4}
NAC:CdS (423 nm)	1.5×10^{-4}	1.5×10^{-4}

are no significant changes in the magnitude of chirality when probing thiolate vs thiol coordination on the surface of the QDs. While there was no increase in the magnitude of chirality at this transition, we did observe more than a 2-fold increase in the *g*-factor magnitude of NAC:CdS vs ELP:CdS. Previously, Puri et al. reported that CdSe QDs with chiral dicarboxylic acid surface ligands can increase *g*-factors by 30-fold when compared to their monocarboxylic acid counterparts, which they attribute to the additional chiral center in the dicarboxylic acid.[37] Since V96-Cys, V54-Cys, and NAC have 289, 163, and one chiral carbon centers, respectively, we expected to see an increase in the *g*-factor proportional to ligand length, which was not observed. However, due to the steric bulk of the ELPs compared to NAC we assume the surface ligand coverage is likely not the same between samples, making this comparison difficult.

The ELP ligand exchange can also be monitored through changes in the hydrodynamic diameter of the ligand:CdS conjugate using DLS (Figure 5). After exchanging the hydrophobic oleate:CdS with glycine, the hydrodynamic diameter decreases from 11.5 ± 2.5 to 6.7 ± 0.5 nm, consistent with a decrease in ligand length from oleate to

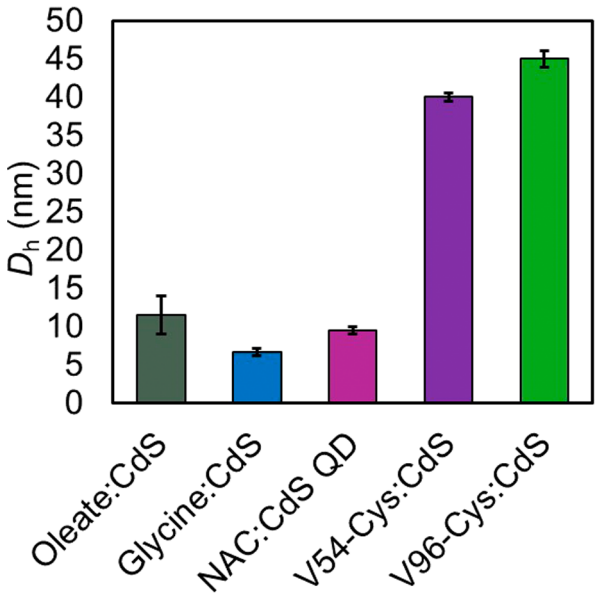

Figure 5. Average hydrodynamic diameter of CdS QDs with corresponding ligands as determined by DLS at 20 °C. The oleate:CdS was measured in toluene, while the remaining samples were measured in water at pH 7.

glycine. Once the glycine:CdS is exchanged with V54-Cys and V96-Cys, the hydrodynamic diameter increases to 40 ± 0.5 and 45 ± 1.1 nm, respectively. These data are also in agreement with the larger hydrodynamic diameter of V96-Cys (10.5 ± 1.0 nm) relative to that of V54-Cys (8.4 ± 0.6 nm) (Figure S9).

Reversible ELP:CdS QD Thermoresponsive Coacervation. The thermoresponsiveness of ELPs makes them attractive ligands for the synthesis of reconfigurable organic−inorganic hybrid materials. The most common example of these types of systems is ELP:gold nanoparticle conjugates.[28,30,52−57] Recently, V96-Cys ELP was successfully conjugated to 20 and 60 nm gold nanoparticles, with the ELP's dynamic coacervation resulting in red-shifted gold plasmonic absorbance features.[28] While ELP:CdSe nanostructures have been reported,[58] no information was provided on the dynamic coacervation of the hybrid material. In this section, we discuss the measured spectroscopic temperature response of V54-Cys:CdS and compare the V96-Cys:CdS and V54-Cys:CdS systems using SAXS. We note that a stark increase in turbidity accompanies spatial rearrangement during coacervation. Thus, the influence of coacervation on the optical properties of QDs cannot be studied in detail. Both V96-Cys:CdS and V54-Cys:CdS collapse into QD-dense coacervates when heated above the ELP transition temperatures, which are 32 °C[28] and 38 °C (Figure S10), respectively. While both V96-Cys:CdS and V54-Cys:CdS assemble, the spectroscopic response of the V54-Cys:CdS variant will be highlighted. For details on the thermoresponsive spectroscopic characterization of the V96-Cys:CdS system, see the Supporting Information (Figures S11, S12, and S22).

Variable-temperature DLS spectra of V54-Cys:CdS show that the particle-dense coacervates produced at 45 °C have an average size of 397 ± 4 nm and that they transition back to ELP-decorated QDs 50 ± 1 nm in average size upon incubation at 20 °C. This temperature-driven assembly−disassembly process is highly reproducible for at least three

https://doi.org/10.1021/acs.langmuir.4c04339
Langmuir 2025, 41, 1047−1056

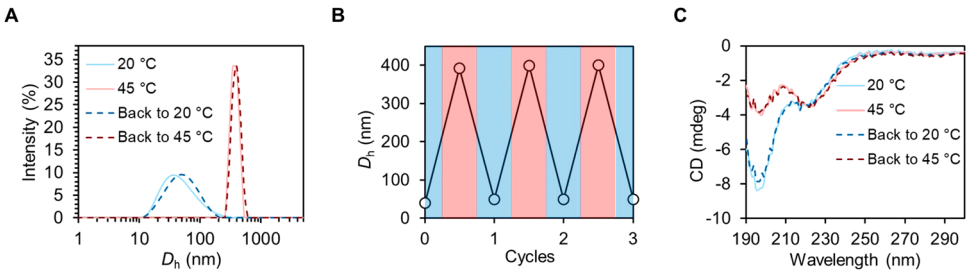

Figure 6. (A) Variable-temperature DLS spectra of V54-Cys:CdS and (B) corresponding hydrodynamic diameter during temperature cycling. (C) Deep-UV variable-temperature CD spectra of V54-Cys:CdS.

heating and cooling cycles (Figure 6A,B). ELP-mediated clustering of QDs is also observed upon incubation of V96-Cys:CdS samples at 40 °C with larger coacervates (510 ± 2 nm) produced above the transition temperature and an average size of 53 ± 2 nm after a return to 20 °C. Like V54-Cys:CdS, the V96-Cys:CdS system also exhibits robust thermoreversibility over multiple heating and cooling cycles (Figure S11). Notably, for both V96-Cys:CdS and V54-Cys:CdS, the average particle size after the first cycle at 20 °C is slightly larger than the original, consistent with hysteresis observed in similar dynamic polymer−nanoparticle systems.[28,59,60]

While DLS gives us insight into coacervate size, variable-temperature CD of dilute (see SI) ELP:CdS provides information about secondary structure changes of the polypeptide bound to the QDs in solution. At 20 °C, ELP:CdS exhibits a strong negative CD signal at 196 nm, and when heated above the ELP transition temperature, the CD magnitude at 196 and 209 nm decreases (Figure 6C and Figure S12). The literature suggests that this corresponds to the conversion of polyproline II-like helical structures to β-structures during coacervation.[57,61−63] These secondary structure changes are also observed for the coacervation of the native ELP (Figures S13 and S14). Unfortunately, the turbidity of the ELP:CdS coacervates makes it difficult to observe spectroscopic changes at visible wavelengths in these samples (Figures S15−S20).

SAXS profiles reveal the presence of QDs in V96-Cys:CdS and V54-Cys:CdS coacervates in the solution phase. The initial measurements of the V96-Cys:CdS and V54-Cys:CdS samples were taken at 20 °C (Figure 7A) and fit to a core−shell sphere model[64] revealing QDs 4.6 nm in diameter, with a shell thickness of 8.6 nm for V96-Cys:CdS and 6.2 nm for V54-Cys:CdS, respectively. (For further explanation including assumptions and limitations of the core−shell sphere model, see the SI.) When the ELP:CdS solutions are heated above

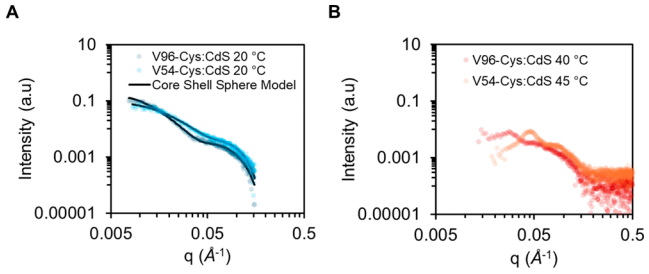

Figure 7. (A) Scattering curves of V96-Cys:CdS (gray) and V54-Cys:CdS (blue) at 20 °C. The core−shell model was used to fit both curves (black line). (B) Scattering curves of V96-Cys:CdS (red) and V54-Cys:CdS at 40 and 45 °C, respectively.

their transition temperatures, distinct scattering features are observed in both ELP:CdS samples (Figure 7B) that are not present in the glycine:CdS samples (Figure S21). These peaks imply a dense CdS QD particle packing mediated by the coacervated ELPs that decorate their surface. Fitting coacervated samples of V96-Cys:CdS and V54-Cys:CdS using a broad peak model reveals interparticle distances of 22.9 and 13.7 nm, respectively. The distance discrepancies of the ELP:CdS systems are rationalized by the ligand shell thickness of V96-Cys:CdS (8.6 nm) and V54-Cys:CdS (6.2 nm). These systems were also tested for reversibility by collecting scattering curves at 20 °C after coacervation. The V96-Cys:CdS QD scattering curve at 20 °C after cycling to 40 °C is similar to the original 20 °C curve (Figure S22), demonstrating reversible coacervation. However, the V54-Cys:CdS samples displayed less reversibility based on the scattering curve at 20 °C after heating to 45 °C (Figure S23). These differences are consistent with the DLS measurements taken at 20 °C after heating the V96-Cys:CdS and V54-Cys:CdS systems (Figure S11 and Figure 6A, blue dashed lines), where the V96-Cys:CdS system has a narrower size population distribution than V54-Cys:CdS after heat cycling. These differences in reversibility indicate ELP-dependent hysteresis in the assembly/disassembly of this organic−inorganic hybrid material, which we hypothesize may be due to (1) differences in the polypeptide:QD size ratios (∼1.9 for V96-Cys:CdS and ∼1.3 for V54-Cys:CdS) and (2) differences in the hydrophobicity of ELPs with the change in length. The second point is corroborated by Unsworth and co-workers, who found an inverse relationship between chain length and hysteresis.[65] Moving forward, the length of the ELPs should be considered for the rational design of these thermally responsive hybrid materials.

Finally, the structure of the V54-Cys:CdS particle-dense coacervate was investigated by (S)TEM (Figure 8). Images of the V96-Cys:CdS coacervates are provided in the Supporting Information (Figure S24). Below the ELP transition temperature, V54-Cys:CdS particles are relatively dispersed and do not show interparticle close-packing on the TEM grid (Figure 8A). QDs with relatively short ligands, such as the oleate:CdS or glycine:CdS (Figure 1), exhibit close-packing on the TEM grid, and the absence of this effect for V54-Cys:CdS can be rationalized by the relatively large size of the ELP ligand. To confirm the structure of the coacervate, V54-Cys:CdS was incubated above the transition temperature and prepared for electron microscopy (see methods). Bright-field TEM reveals quasispherical coacervates of around 500 nm in diameter composed of dense QDs presumably held together by coacervated ELP ligands (Figure 8B). Scanning TEM reveals the organic ELP component at a higher contrast, observed as a

https://doi.org/10.1021/acs.langmuir.4c04339
Langmuir 2025, 41, 1047−1056

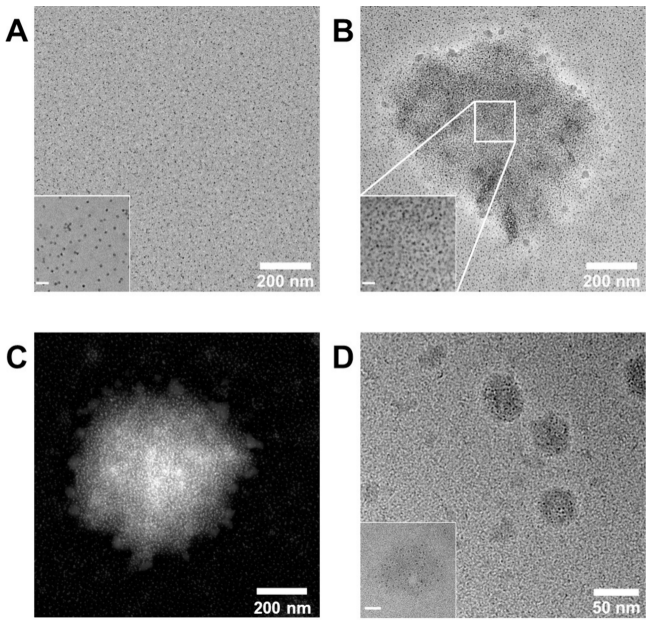

Figure 8. TEM images of V54-Cys:CdS prepared at (A) 20 °C and (B) 45 °C. (C) Scanning TEM image of V54-Cys:CdS prepared at 45 °C. (D) Cryogenic TEM images of V54-Cys:CdS prepared at 45 °C. Higher-magnification insets have a 20 nm scale bar.

white haze surrounding the QDs within the coacervate (Figure 8C). The coacervate is decorated by small organic structures about 15−35 nm in diameter, seen both in the bright-field TEM and scanning TEM images, and these are assigned to QD-free ELP clusters. Higher-magnification images of the coacervates (Figure 8B, inset) reveal individual QDs within the coacervate. It is worth noting that the QDs are not ordered in the dried coacervate and cryogenic TEM images (Figure 8D) of small coacervates also do not show ordering.

CONCLUSIONS

We have developed a two-step ligand exchange method to bind V96-Cys and V54-Cys ELPs to CdS QDs. The exchange is confirmed using CD spectroscopy in the visible light region by observing a chiral absorbance corresponding to the excitonic transitions of the CdS QD. By comparing the chirality-induced CD response for a range of small-molecule model ligands, including NAC, L-Cys, and L-Cys-Me, V96-Cys and V54-Cys were determined to bind to CdS QDs through the C-terminal cysteine residue preferentially. This is the first literature example of postsynthetically inducing exciton chirality in QDs using proteins or polypeptides. Notably, we were able to identify the amino acid bound to the QD surface using μM polypeptide concentrations compared to mM or higher concentrations previously used with L-Cys and QDs for NMR studies. This highlights the advantage of using CD to probe protein−QD surface interactions, particularly in biologically relevant environments where the protein concentration is limited by solubility. Additionally, for the first time, we reported the reversible coacervation of ELP:CdS by DLS and CD spectroscopies and confirmed the coacervate structure through (S)TEM. Moreover, the analysis of SAXS data revealed increased spatial ordering of CdS QDs in both V96-Cys:CdS and V54-Cys:CdS systems, highlighting the ELP's ability to drive assembly in these hybrid materials. This study demonstrates the usefulness of circular dichroism in determining the success of biological ligand exchange on quantum dots. We believe that this technique can be applied to a diverse set of bioligand:QD systems in the future. Furthermore, leveraging the knowledge gained in this study about the ELP:QD surface interaction, we aim to study more complex inorganic nanostructures conjugated with ELPs that dynamically coacervate in a manner that exploits both the properties of the ELP and the inorganic nanostructure to access a broad library of functional hybrid materials with emergent functionality.

ASSOCIATED CONTENT

Supporting Information

The Supporting Information is available free of charge at https://pubs.acs.org/doi/10.1021/acs.langmuir.4c04339.

Additional spectroscopic, microscopic, and analytical data (PDF)

AUTHOR INFORMATION

Corresponding Author

Brandi M. Cossairt − *Department of Chemistry, University of Washington, Seattle, Washington 98195, United States;* orcid.org/0000-0002-9891-3259; Email: cossairt@uw.edu

Authors

Christopher D. Lowe − *Department of Chemistry, University of Washington, Seattle, Washington 98195, United States*

Helen C. Larson − *Department of Chemistry, University of Washington, Seattle, Washington 98195, United States*

Yifeng Cai − *Department of Chemical Engineering, University of Washington, Seattle, Washington 98195, United States*

Huat Thart Chiang − *Department of Chemical Engineering, University of Washington, Seattle, Washington 98195, United States;* orcid.org/0000-0002-0042-7958

Lilo D. Pozzo − *Department of Chemical Engineering, University of Washington, Seattle, Washington 98195, United States;* orcid.org/0000-0001-7104-9061

François Baneyx − *Department of Chemical Engineering, University of Washington, Seattle, Washington 98195, United States;* orcid.org/0000-0001-5596-7903

Complete contact information is available at: https://pubs.acs.org/10.1021/acs.langmuir.4c04339

Author Contributions

#H.C.L. and Y.C. contributed equally.

Notes

The authors declare no competing financial interest.

ACKNOWLEDGMENTS

We are grateful to Dr. Jinrong Ma for helping to construct the plasmids used in this study. Additionally, we are grateful to Dr. Martin Sadilek and Brandon Bol for their help analyzing circular dichroism spectra. We would also like to thank Emily Miura-Stempel for her revision contributions. This material was based upon work supported by the U.S. Department of Energy, Office of Science, Office of Basic Energy Sciences, as part of the Energy Frontier Research Centers program (CSSAS − The Center for the Science of Synthesis Across Scales under award number DE-SC0019288). Part of this work was conducted at the Molecular Analysis Facility, a National Nanotechnology Coordinated Infrastructure (NNCI) site at

the University of Washington, which is supported in part by funds from the National Science Foundation (awards NNCI-2025489 and NNCI-1542101), the Molecular Engineering & Sciences Institute, and the Clean Energy Institute. Part of this work was conducted using instrumentation funded by the University of Washington Student Technology Fee. The authors acknowledge the use of facilities and instrumentation supported by the U.S. National Science Foundation through the Major Research Instrumentation (MRI) program (DMR-2116265) and the UW Molecular Engineering Materials Center (MEM-C), a Materials Research Science and Engineering Center (DMR-2308979). This work benefited from the use of the SasView application, originally developed under NSF award DMR-0520547. SasView contains code developed with funding from the European Union's Horizon 2020 research and innovation program under the SINE2020 project, grant agreement no. 654000.

REFERENCES

(1) Tohgha, U.; Varga, K.; Balaz, M. Achiral CdSe Quantum Dots Exhibit Optical Activity in the Visible Region upon Post-Synthetic Ligand Exchange with D- or L-Cysteine. *Chem. Commun.* **2013**, *49* (18), 1844−1846.
(2) Tohgha, U.; Deol, K. K.; Porter, A. G.; Bartko, S. G.; Choi, J. K.; Leonard, B. M.; Varga, K.; Kubelka, J.; Muller, G.; Balaz, M. Ligand Induced Circular Dichroism and Circularly Polarized Luminescence in CdSe Quantum Dots. *ACS Nano* **2013**, *7* (12), 11094−11102.
(3) Moloney, M. P.; Gun'ko, Y. K.; Kelly, J. M. Chiral Highly Luminescent CdS Quantum Dots. *Chem. Commun.* **2007**, *38*, 3900−3902.
(4) Elliott, S. D.; Moloney, M. P.; Gun'ko, Y. K. Chiral Shells and Achiral Cores in CdS Quantum Dots. *Nano Lett.* **2008**, *8* (8), 2452−2457.
(5) Zhou, Y.; Yang, M.; Sun, K.; Tang, Z.; Kotov, N. A. Similar Topological Origin of Chiral Centers in Organic and Nanoscale Inorganic Structures: Effect of Stabilizer Chirality on Optical Isomerism and Growth of CdTe Nanocrystals. *J. Am. Chem. Soc.* **2010**, *132* (17), 6006−6013.
(6) Ben-Moshe, A.; Teitelboim, A.; Oron, D.; Markovich, G. Probing the Interaction of Quantum Dots with Chiral Capping Molecules Using Circular Dichroism Spectroscopy. *Nano Lett.* **2016**, *16* (12), 7467−7473.
(7) Han, P.; Du, T.; Yang, X.; Zhao, Y.; Zhou, S.; Zhao, J. Optical Activity and Excitonic Characteristics of Chiral CdSe Quantum Dots. *J. Phys. Chem. Lett.* **2024**, *15* (12), 3249−3257.
(8) Dameron, C. T.; Winge, D. R. Characterization of Peptide-Coated Cadmium-Sulfide Crystallites. *Inorg. Chem.* **1990**, *29* (7), 1343−1348.
(9) Monahan, M.; Cai, B.; Jian, T.; Zhang, S.; Zhu, G.; Chen, C.-L.; Yoreo, J. J. D.; Cossairt, B. M. Peptoid-Directed Assembly of CdSe Nanoparticles. *Nanoscale* **2021**, *13* (2), 1273−1282.
(10) Monahan, M.; Homer, M.; Zhang, S.; Zheng, R.; Chen, C.-L.; De Yoreo, J.; Cossairt, B. M. Impact of Nanoparticle Size and Surface Chemistry on Peptoid Self-Assembly. *ACS Nano* **2022**, *16* (5), 8095−8106.
(11) Ma, N.; Yang, J.; Stewart, K. M.; Kelley, S. O. DNA-Passivated CdS Nanocrystals: Luminescence, Bioimaging, and Toxicity Profiles. *Langmuir* **2007**, *23* (26), 12783−12787.
(12) Gil, H. M.; Price, T. W.; Chelani, K.; Bouillard, J.-S. G.; Calaminus, S. D. J.; Stasiuk, G. J. NIR-Quantum Dots in Biomedical Imaging and Their Future. *iScience* **2021**, *24* (3), No. 102189.
(13) Garai-Ibabe, G.; Saa, L.; Pavlov, V. Enzymatic Product-Mediated Stabilization of CdS Quantum Dots Produced In Situ: Application for Detection of Reduced Glutathione, NADPH, and Glutathione Reductase Activity. *Anal. Chem.* **2013**, *85* (11), 5542−5546.
(14) Probst, C. E.; Zrazhevskiy, P.; Bagalkot, V.; Gao, X. Quantum Dots as a Platform for Nanoparticle Drug Delivery Vehicle Design. *Inorg. Nanoparticle Platf.* **2013**, *65* (5), 703−718.
(15) Sun, M.; Xu, L.; Qu, A.; Zhao, P.; Hao, T.; Ma, W.; Hao, C.; Wen, X.; Colombari, F. M.; de Moura, A. F.; Kotov, N. A.; Xu, C.; Kuang, H. Site-Selective Photoinduced Cleavage and Profiling of DNA by Chiral Semiconductor Nanoparticles. *Nat. Chem.* **2018**, *10* (8), 821−830.
(16) Urry, D. W. Free Energy Transduction in Polypeptides and Proteins Based on Inverse Temperature Transitions. *Prog. Biophys. Mol. Biol.* **1992**, *57* (1), 23−57.
(17) Urry, D. W.; Long, M. M.; Cox, B. A.; Ohnishi, T.; Mitchell, L. W.; Jacobs, M. The Synthetic Polypentapeptide of Elastin Coacervates and Forms Filamentous Aggregates. *Biochim. Biophys. Acta BBA - Protein Struct.* **1974**, *371* (2), 597−602.
(18) Roberts, S.; Dzuricky, M.; Chilkoti, A. Elastin-like Polypeptides as Models of Intrinsically Disordered Proteins. *FEBS Lett.* **2015**, *589* (19 Part A), 2477−2486.
(19) McDaniel, J. R.; MacKay, J. A.; Quiroz, F. G.; Chilkoti, A. Recursive Directional Ligation by Plasmid Reconstruction Allows Rapid and Seamless Cloning of Oligomeric Genes. *Biomacromolecules* **2010**, *11* (4), 944−952.
(20) Rodríguez-Cabello, J. C.; Arias, F. J.; Rodrigo, M. A.; Girotti, A. Elastin-like Polypeptides in Drug Delivery. *Adv. Drug Delivery Rev.* **2016**, *97*, 85−100.
(21) Kostal, J.; Mulchandani, A.; Chen, W. Tunable Biopolymers for Heavy Metal Removal. *Macromolecules* **2001**, *34* (7), 2257−2261.
(22) Mullerpatan, A.; Chandra, D.; Kane, E.; Karande, P.; Cramer, S. Purification of Proteins Using Peptide-ELP Based Affinity Precipitation. *J. Biotechnol.* **2020**, *309*, 59−67.
(23) Nettles, D. L.; Chilkoti, A.; Setton, L. A. Applications of Elastin-like Polypeptides in Tissue Engineering. *Adv. Drug Delivery Rev.* **2010**, *62* (15), 1479−1485.
(24) Shao, L.; Ma, J.; Prelesnik, J. L.; Zhou, Y.; Nguyen, M.; Zhao, M.; Jenekhe, S. A.; Kalinin, S. V.; Ferguson, A. L.; Pfaendtner, J.; Mundy, C. J.; De Yoreo, J. J.; Baneyx, F.; Chen, C.-L. Hierarchical Materials from High Information Content Macromolecular Building Blocks: Construction, Dynamic Interventions, and Prediction. *Chem. Rev.* **2022**, *122* (24), 17397−17478.
(25) Rosenthal, S. J.; Chang, J. C.; Kovtun, O.; McBride, J. R.; Tomlinson, I. D. Biocompatible Quantum Dots for Biological Applications. *Chem. Biol.* **2011**, *18* (1), 10−24.
(26) Fahmi, A.; Pietsch, T.; Bryszewska, M.; Rodríguez-Cabello, J. C.; Koceva-Chyla, A.; Arias, F. J.; Rodrigo, M. A.; Gindy, N. Fabrication of CdSe-Nanofibers with Potential for Biomedical Applications. *Adv. Funct. Mater.* **2010**, *20* (6), 1011−1018.
(27) Biswas, P.; Cella, L. N.; Kang, S. H.; Mulchandani, A.; Yates, M. V.; Chen, W. A Quantum-Dot Based Protein Module for in Vivo Monitoring of Protease Activity through Fluorescence Resonance Energy Transfer. *Chem. Commun.* **2011**, *47* (18), 5259−5261.
(28) Cai, Y.; Naser, N. Y.; Ma, J.; Baneyx, F. Precision Loading and Delivery of Molecular Cargo by Size-Controlled Coacervation of Gold Nanoparticles Functionalized with Elastin-like Peptides. *Biomacromolecules* **2024**, *25* (4), 2390−2398.
(29) Hamachi, L. S.; Yang, H.; Plante, I. J.-L.; Saenz, N.; Qian, K.; Campos, M. P.; Cleveland, G. T.; Rreza, I.; Oza, A.; Walravens, W.; Chan, E. M.; Hens, Z.; Crowther, A. C.; Owen, J. S. Precursor Reaction Kinetics Control Compositional Grading and Size of CdSe1−xSx Nanocrystal Heterostructures. *Chem. Sci.* **2019**, *10* (26), 6539−6552.
(30) Ma, Q.; Liu, L.; Yang, Z.; Zheng, P. Facile Synthesis of Peptide-Conjugated Gold Nanoclusters with Different Lengths. *Nanomaterials* **2021**, *11* (11), 2932.
(31) Peng, Z. A.; Peng, X. Formation of High-Quality CdTe, CdSe, and CdS Nanocrystals Using CdO as Precursor. *J. Am. Chem. Soc.* **2001**, *123* (1), 183−184.
(32) Bressler, I.; Pauw, B. R.; Thünemann, A. F. McSAS: Software for the Retrieval of Model Parameter Distributions from Scattering Patterns. *J. Appl. Crystallogr.* **2015**, *48* (3), 962−969.

https://doi.org/10.1021/acs.langmuir.4c04339
Langmuir 2025, 41, 1047−1056

(33) Murray, C. B.; Norris, D. J.; Bawendi, M. G. Synthesis and Characterization of Nearly Monodisperse CdE (E = Sulfur, Selenium, Tellurium) Semiconductor Nanocrystallites. *J. Am. Chem. Soc.* **1993**, *115* (19), 8706−8715.
(34) Katari, J. E. B.; Colvin, V. L.; Alivisatos, A. P. X-Ray Photoelectron Spectroscopy of CdSe Nanocrystals with Applications to Studies of the Nanocrystal Surface. *J. Phys. Chem.* **1994**, *98* (15), 4109−4117.
(35) Choi, J. K.; Haynie, B. E.; Tohgha, U.; Pap, L.; Elliott, K. W.; Leonard, B. M.; Dzyuba, S. V.; Varga, K.; Kubelka, J.; Balaz, M. Chirality Inversion of CdSe and CdS Quantum Dots without Changing the Stereochemistry of the Capping Ligand. *ACS Nano* **2016**, *10* (3), 3809−3815.
(36) Varga, K.; Tannir, S.; Haynie, B. E.; Leonard, B. M.; Dzyuba, S. V.; Kubelka, J.; Balaz, M. CdSe Quantum Dots Functionalized with Chiral, Thiol-Free Carboxylic Acids: Unraveling Structural Requirements for Ligand-Induced Chirality. *ACS Nano* **2017**, *11* (10), 9846−9853.
(37) Puri, M.; Ferry, V. E. Circular Dichroism of CdSe Nanocrystals Bound by Chiral Carboxylic Acids. *ACS Nano* **2017**, *11* (12), 12240−12246.
(38) Joh, Y. A.; Kwon, Y. H.; Tannir, S.; Leonard, B. M.; Kubelka, J.; Varga, K.; Balaz, M. The Effect of Molecular Isomerism on the Induced Circular Dichroism of Cadmium Sulfide Quantum Dots. *J. Mater. Chem. C* **2021**, *9* (48), 17483−17495.
(39) Kwon, Y. H.; Joh, Y. A.; Leonard, B. M.; Balaz, M.; Varga, K. Threonine Functionalized Colloidal Cadmium Sulfide (CdS) Quantum Dots: The Role of Solvent and Counterion in Ligand Induced Chiroptical Properties. *J. Colloid Interface Sci.* **2023**, *642*, 771−778.
(40) Baldwin, R. L. How Hofmeister Ion Interactions Affect Protein Stability. *Biophys. J.* **1996**, *71* (4), 2056−2063.
(41) Kunz, W.; Henle, J.; Ninham, B. W. 'Zur Lehre von Der Wirkung Der Salze' (about the Science of the Effect of Salts): Franz Hofmeister's Historical Papers. *Curr. Opin. Colloid Interface Sci.* **2004**, *9* (1), 19−37.
(42) Ma, L.; Tu, C.; Le, P.; Chitoor, S.; Lim, S. J.; Zahid, M. U.; Teng, K. W.; Ge, P.; Selvin, P. R.; Smith, A. M. Multidentate Polymer Coatings for Compact and Homogeneous Quantum Dots with Efficient Bioconjugation. *J. Am. Chem. Soc.* **2016**, *138* (10), 3382−3394.
(43) Zhang, H.; Chen, J.; Xiao, C.; Tao, Y.; Wang, X. A Multifunctional Polypeptide via Ugi Reaction for Compact and Biocompatible Quantum Dots with Efficient Bioconjugation. *Bioconjugate Chem.* **2018**, *29* (4), 1335−1343.
(44) Susumu, K.; Oh, E.; Delehanty, J. B.; Pinaud, F.; Gemmill, K. B.; Walper, S.; Breger, J.; Schroeder, M. J.; Stewart, M. H.; Jain, V.; Whitaker, C. M.; Huston, A. L.; Medintz, I. L. A New Family of Pyridine-Appended Multidentate Polymers As Hydrophilic Surface Ligands for Preparing Stable Biocompatible Quantum Dots. *Chem. Mater.* **2014**, *26* (18), 5327−5344.
(45) Jin, Z.; Dridi, N.; Palui, G.; Palomo, V.; Jokerst, J. V.; Dawson, P. E.; Sang, Q.-X. A.; Mattoussi, H. Quantum Dot−Peptide Conjugates as Energy Transfer Probes for Sensing the Proteolytic Activity of Matrix Metalloproteinase-14. *Anal. Chem.* **2023**, *95* (5), 2713−2722.
(46) Danehy, J. P.; Noel, C. J. The Relative Nucleophilic Character of Several Mercaptans toward Ethylene Oxide1. *J. Am. Chem. Soc.* **1960**, *82* (10), 2511−2515.
(47) Kuznetsova, V. A.; Mates-Torres, E.; Prochukhan, N.; Marcastel, M.; Purcell-Milton, F.; O'Brien, J.; Visheratina, A. K.; Martinez-Carmona, M.; Gromova, Y.; Garcia-Melchor, M.; Gun'ko, Y. K. Effect of Chiral Ligand Concentration and Binding Mode on Chiroptical Activity of CdSe/CdS Quantum Dots. *ACS Nano* **2019**, *13* (11), 13560−13572.
(48) Kurihara, T.; Noda, Y.; Takegoshi, K. Capping Structure of Ligand−Cysteine on CdSe Magic-Sized Clusters. *ACS Omega* **2019**, *4* (2), 3476−3483.
(49) Fazary, A. E.; Awwad, N. S.; Ibrahium, H. A.; Shati, A. A.; Alfaifi, M. Y.; Ju, Y.-H. Protonation Equilibria of N-Acetylcysteine. *ACS Omega* **2020**, *5* (31), 19598−19605.
(50) Jalilehvand, F.; Amini, Z.; Parmar, K.; Kang, E. Y. Cadmium(II) N-Acetylcysteine Complex Formation in Aqueous Solution. *Dalton Trans.* **2011**, *40* (47), 12771−12778.
(51) Anderson, N. C.; Hendricks, M. P.; Choi, J. J.; Owen, J. S. Ligand Exchange and the Stoichiometry of Metal Chalcogenide Nanocrystals: Spectroscopic Observation of Facile Metal-Carboxylate Displacement and Binding. *J. Am. Chem. Soc.* **2013**, *135* (49), 18536−18548.
(52) Lin, Y.; Xia, X.; Wang, M.; Wang, Q.; An, B.; Tao, H.; Xu, Q.; Omenetto, F.; Kaplan, D. L. Genetically Programmable Thermoresponsive Plasmonic Gold/Silk-Elastin Protein Core/Shell Nanoparticles. *Langmuir* **2014**, *30* (15), 4406−4414.
(53) Nath, N.; Chilkoti, A. Interfacial Phase Transition of an Environmentally Responsive Elastin Biopolymer Adsorbed on Functionalized Gold Nanoparticles Studied by Colloidal Surface Plasmon Resonance. *J. Am. Chem. Soc.* **2001**, *123* (34), 8197−8202.
(54) Alvarez-Rodriguez, R.; Alonso, M.; Girotti, A.; Reboto, V.; Rodriguez-Cabello, J. C. One-Pot Synthesis of pH and Temperature Sensitive Gold Clusters Mediated by a Recombinant Elastin-like Polymer. *Eur. Polym. J.* **2010**, *46* (4), 643−650.
(55) Huang, H.-C.; Koria, P.; Parker, S. M.; Selby, L.; Megeed, Z.; Rege, K. Optically Responsive Gold Nanorod−Polypeptide Assemblies. *Langmuir* **2008**, *24* (24), 14139−14144.
(56) Zong, J.; Cobb, S. L.; Cameron, N. R. Short Elastin-like Peptide-Functionalized Gold Nanoparticles That Are Temperature Responsive under near-Physiological Conditions. *J. Mater. Chem. B* **2018**, *6* (41), 6667−6674.
(57) Higashi, N.; Ochiai, T.; Kanazawa, C.; Koga, T. Site-Specific Adsorption of Gold Nanoparticles Coated with Thermo-Responsive Peptides. *Polym. J.* **2013**, *45* (5), 523−528.
(58) Fahmi, A.; Pietsch, T.; Bryszewska, M.; Rodriguez-Cabello, J. C.; Koceva-Chyla, A.; Javier Arias, F.; Alonso Rodrigo, M.; Gindy, N. Fabrication of CdSe-Nanofibers with Potential for Biomedical Applications. *Adv. Funct. Mater.* **2010**, *20* (6), 1011−1018.
(59) Qian, Z.; Guye, K. N.; Masiello, D. J.; Ginger, D. S. Dynamic Optical Switching of Polymer/Plasmonic Nanoparticle Hybrids with Sparse Loading. *J. Phys. Chem. B* **2017**, *121* (5), 1092−1099.
(60) Ding, T.; Valev, V. K.; Salmon, A. R.; Forman, C. J.; Smoukov, S. K.; Scherman, O. A.; Frenkel, D.; Baumberg, J. J. Light-Induced Actuating Nanotransducers. *Proc. Natl. Acad. Sci. U. S. A.* **2016**, *113* (20), 5503−5507.
(61) Sumiyoshi, S.; Suyama, K.; Tanaka, N.; Andoh, T.; Nagata, A.; Tomohara, K.; Taniguchi, S.; Maeda, I.; Nose, T. Development of Truncated Elastin-like Peptide Analogues with Improved Temperature-Response and Self-Assembling Properties. *Sci. Rep.* **2022**, *12* (1), No. 19414.
(62) Brahms, S.; Brahms, J.; Spach, G.; Brack, A. Identification of Beta,Beta-Turns and Unordered Conformations in Polypeptide Chains by Vacuum Ultraviolet Circular Dichroism. *Proc. Natl. Acad. Sci. U. S. A.* **1977**, *74* (8), 3208−3212.
(63) Urry, D. W. Physical Chemistry of Biological Free Energy Transduction As Demonstrated by Elastic Protein-Based Polymers. *J. Phys. Chem. B* **1997**, *101* (51), 11007−11028.
(64) Rice, S. A. Small Angle Scattering of X-Rays. A. Guinier and G. Fournet. Translated by C. B. Wilson and with a Bibliographical Appendix by K. L. Yudowitch. Wiley, New York, 1955. 268 Pp. *J. Polym. Sci.* **1956**, *19* (93), 594−594.
(65) Bahniuk, M. S.; Alshememry, A. K.; Elgersma, S. V.; Unsworth, L. D. Self-Assembly/Disassembly Hysteresis of Nanoparticles Composed of Marginally Soluble, Short Elastin-like Polypeptides. *J. Nanobiotechnology* **2018**, *16* (1), 15.

https://doi.org/10.1021/acs.langmuir.4c04339
Langmuir 2025, 41, 1047−1056